Available online at www.sciencedirect.com
ScienceDirect
Trans. Nonferrous Met. Soc. China 30(2020) 1605−1614
Transactions of Nonferrous Metals Society of China
www.tnmsc.cn

Morphology controlled synthesis of ZnO nanoparticles for in-vitro evaluation of antibacterial activity

Naila ZUBAIR, Khalida AKHTAR

National Center of Excellence in Physical Chemistry, University of Peshawar, Peshawar-25120, Khyber Pukhtoonkhwa, Pakistan

Received 12 June 2019; accepted 20 April 2020

Abstract: Novel hierarchical flower- and nanorod-shaped ZnO nanoparticles with uniform morphological features were successfully synthesized through controlled precipitation method in aqueous media without using any surfactant or template. To elucidate the growth mechanism of the synthesized nanoparticles, the effects of pH, reaction time and temperature were studied systematically. Selected ZnO samples were then subjected to SEM, FT-IR and XRD analysis. XRD patterns confirmed well crystalline nature of the as-synthesized powders. Furthermore, synthesized nanoparticles (hierarchical flowers as ZnO-1 and nanorods as ZnO-2), as well as commercial ZnO (ZnO-Com), were then investigated for in-vitro evaluation of antibacterial activity against various bacterial strains of clinical importance. Results showed that ZnO-2 exhibited higher antibacterial activity to all tested strains than ZnO-1, while ZnO-Com showed no antibacterial response in the applied experimental conditions. In addition, ZnO concentration-dependent antibacterial study unfolded that size of inhibition zones increased significantly from ~30 to 33 mm against *Streptococcus mutans* and from ~28 to 30 mm against *Escherichia coli* with increasing ZnO-2 concentration from 0.25 to 0.75 μg/μL. The present study, therefore, suggests that the application of synthesized ZnO nanoparticles as the antibacterial agent may be effective for inhibiting certain pathogenic bacteria in biomedical sides.
Key words: ZnO; nanoparticles; bacterial strain; antibacterial activity

1 Introduction

Uniform fine particles of zinc oxide have emerged as the foremost multifunctional materials due to the remarkable performance in a number of high-tech applications, such as gas sensors, catalysis, cosmetics, food preservation, and nanomedicines [1−5]. In particular, zinc oxide being a versatile compound, is of prime importance due to its unique properties, like good electrical conductivity, enhanced UV protection, biocompatibility, and excellent antimicrobial activity [6−8]. Besides, zinc oxide offers remarkable benefits in biomedical and clinical sites due to significant antibacterial activities over broad-spectrum pathogenic bacteria. It has been revealed as a promising candidate for orthopedic and dental implant coating [8].

Since antibacterial activity is one of the existing hot research programs, it has attracted considerable interest in nanomedicine to fulfill the drug delivery requirements, to minimize antibiotic concentration and to control drug-resistant pathogenic bacteria. As such, the introduction of a novel and a powerful antibacterial agent is of vital importance to control pathogenic bacteria. In this respect, it has been reported that ZnO could be effectively used as an antibacterial agent because of its biocompatible nature and high purity. Besides, it shows no resistance against antibiotics [9]. It has been used as an antibacterial agent in both nano and microscale formulations. The toxicity perspective revealed that ZnO nanoparticles exhibit selective

Corresponding author: Khalida AKHTAR; E-mail: khalida_akhtar@yahoo.com
DOI: 10.1016/S1003-6326(20)65323-7

toxicity towards bacteria with no harmful effects on human cells [10]. It has been suggested that on contact with bacteria, the cytotoxic effects of ZnO nanoparticles primarily disrupt the cell membrane, resulting in subsequent leakage of intracellular contents and thus cell death. Being a biosafe material, it is also used as an antibacterial agent in the food packaging industry, against various food-born diseases. ZnO nanoparticles are appropriately incorporated in the packaging materials, where they interact with pathogenic bacteria on the food surface, causing inhibition of cell growth and eventually bacterial death [11].

A comparative study [12] for examining the antibacterial activity of CuO, ZnO and Fe_2O_3 revealed that ZnO showed the most significant inhibitory effects against various bacterial species. The authors explored that ZnO nanoparticles possess the potential to be used as an antibacterial agent against different pathogenic bacteria. THOMAS et al [13] prepared ZnO by using a stabilizing agent, sodium dodecyl sulfate. They evaluated the antibacterial activity of both bulk and nanoparticle over a broad spectrum of bacterial species. They observed that the nanoparticle of ZnO produced better results than the bulk ZnO and hence reported that antibacterial activity increased with the decrease in particle size of the agent.

In the present work, uniform fine particles of ZnO with controlled morphological features were synthesized in aqueous media using the straightforward and economically feasible method. The synthesized ZnO, as well as commercially available ZnO powders, were then employed for antibacterial activity against various pathogenic bacteria to check the effect of particle uniformity and morphology on the antibacterial performance of the test material.

2 Experimental

2.1 Materials

Zinc nitrate and ammonium hydroxide were purchased from the reputed firms. The bacteriological grade nutrient agar and nutrient broth were also obtained for performing an antibacterial activity. Experiments were conducted using Pyrex glassware. Distilled water was used for making all sorts of solutions.

2.2 Synthesis of ZnO nanoparticles

ZnO uniform nanoparticles were prepared through a controlled precipitation method. For this purpose, the aqueous solution of zinc nitrate (0.1−0.2 mol/L) and ammonium hydroxide (25%) were heated at constant temperatures for 5−30 min time intervals. In some cases, aqueous solutions of zinc nitrate were purged with ammonia gas at the flow rate of 110 mL/min under the same reaction conditions. The precipitated powders were then filtered using vacuum filtration, air-dried and stored for further study.

2.3 Characterization of ZnO nanoparticles

The particle morphology of synthesized powders was examined using a scanning electron microscope (JEOL, JSM−5910). For crystallinity and phase identification, the samples were subjected to X-ray diffractometry (PXRD, JEOL JDX−3532). The FTIR spectroscopic analysis was carried out by using FTIR (Shimadzu; IR Prestige−21 & FTIR 8400S) to determine the composition and presence of the functional group in the test materials.

2.4 Antibacterial activity tests

The antibacterial activity of the selected samples was assessed against the clinical strains of Gram-positive and Gram-negative bacteria (*S. aureus*, *S. mutans*, *E. coli*, *P. aeruginosa*, and *Enterobacter cloacae*) by using agar well diffusion method. The bacterial strains were collected from Khyber Teaching Hospital KPK, Pakistan. Fresh culture of each test microorganism at the concentration of 7.5×10^6 CFU/50 μL was spread over Muller−Hinton agar plates having wells of 8 mm in diameter. Then 20 μL of the desired particle suspensions were added into wells at three different concentrations (0.25, 0.50 and 0.75 μg/μL). Ciprofloxacin was used as a positive control. The plates were incubated overnight at (35±2) °C, and antibacterial activity was examined by measuring zones of inhibition against the test microorganisms.

3 Result and discussion

3.1 Characterization of ZnO nanoparticles

3.1.1 SEM analysis

Uniform and novel ZnO architectures were prepared from heating the aqueous solutions of zinc

nitrate and ammonium hydroxide at constant temperatures. In all cases, ZnO powders in the reactant mixtures were formed from the precipitation reactions that mostly emerged in the aqueous medium. The mechanism of ZnO formation through the reaction of ammonia with dissolved Zn^{2+} ions can be summarized in the following equations [9,14]:

$$NH_3+H_2O\rightleftharpoons NH_4^+ +OH^- \quad (1)$$

$$Zn^{2+}+4NH_3\rightleftharpoons[Zn(NH_3)_4]^{2+}\rightarrow ZnO+4NH_3+2H_2O \quad (2)$$

$$[Zn(NH_3)_4]^{2+}+4OH^-\rightarrow[Zn(OH)_4]^{2-}+4NH_3 \quad (3)$$

$$Zn^{2+}+4OH^-\rightleftharpoons[Zn(OH)_4]^{2-}\rightleftharpoons ZnO+H_2O+2OH^- \quad (4)$$

It is well known that crystal formation is generally controlled by the nucleation and growth rates, which in turn is preceded by the induction time. During the induction period, ammonia provides hydroxyl ions that are used in generating and subsequent development of the primary growth units $[Zn(NH_3)_4]^{2+}$ and $[Zn(OH)_4]^{2-}$ [15]. In our designed experimental conditions, at pH higher than pH_{iep} of ZnO (pH_{iep}≈9.56), Zn^{2+} cations form mainly as $[Zn(OH)_4]^{2-}$ with a small quantity of $[Zn(NH_3)_4]^{2+}$ complex. When zinc nitrate solution was purged with ammonia gas for 30 min with 110 mL/min flow rate at 30 °C, relatively uniform hierarchical 3D ZnO nanoflowers were obtained (Fig. 1). It was of interest to know about the growth mechanism of these appealing flower-like nanostructures. Since it has been investigated that reaction time plays a substantial role during the production and growth of nanoparticles, the same experiment was repeated to understand the effect

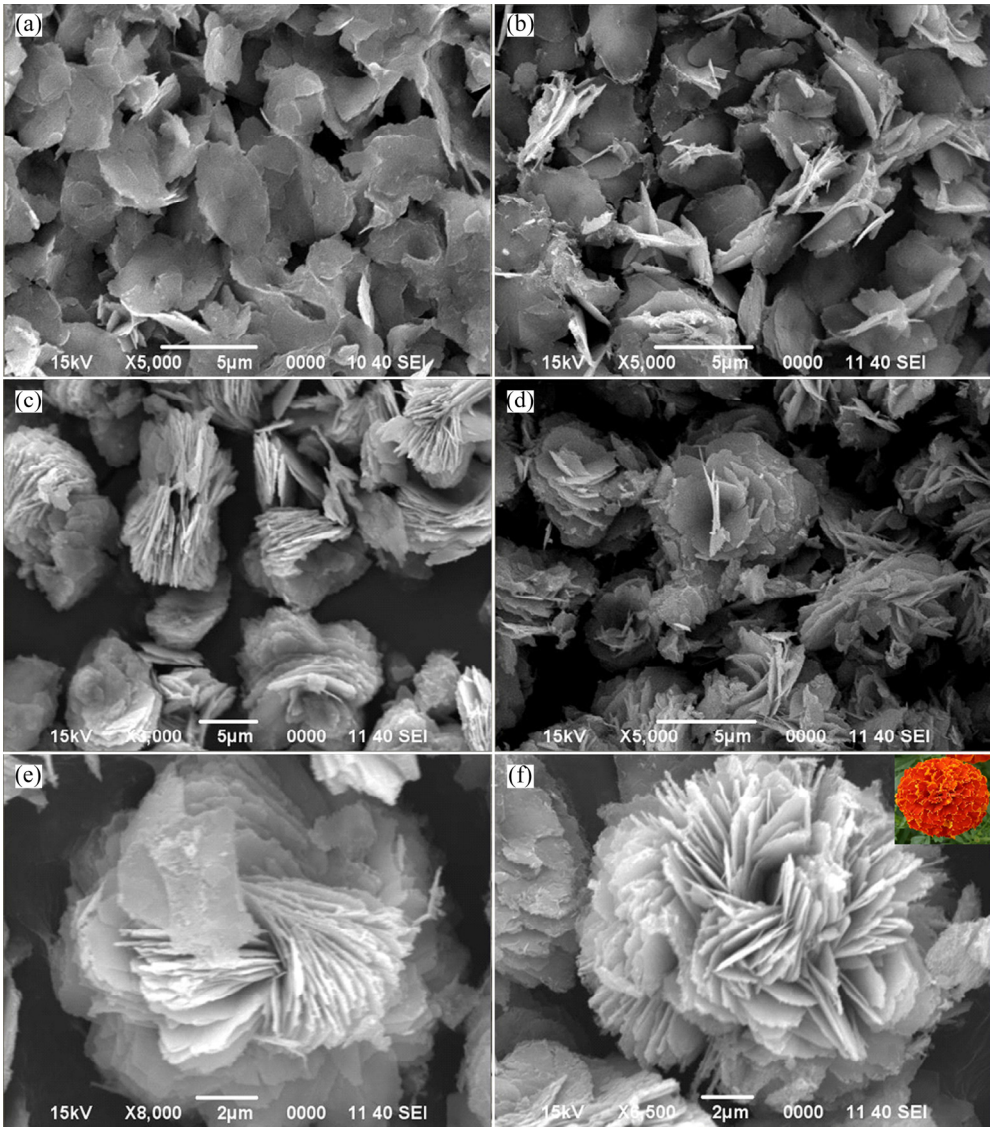

Fig. 1 SEM images of particles synthesized using gaseous ammonia at different time intervals: (a) 5 min; (b) 10 min; (c) 15 min; (d) 20 min; (e) 25 min; (f) 30 min

of reaction time on the particle morphology, and the precipitated powder was isolated after every 5 min and analyzed for morphological characteristics.

Figure 1 shows the whole scenario of successive growth stages of hierarchical flower-like ZnO structures as a function of reaction time (5−30 min). This process of flower formation clearly illustrated the so-called growth process consisting of a fast nucleation stage followed by slow aggregation. As can be seen from the SEM image in Fig. 1(a), initially uniform and well-distributed 2D nanosheet-like petals were produced. When the reaction time exceeded 10 min, the primarily obtained nanopetals attached in a specific manner (Fig. 1(b)). In this way, these nanopetals followed a standard crystallographic orientation and thus reduced their surface energy [16]. It was indicated that as the induction time was increased beyond 5 min, the more growth units, i.e. $[Zn(OH)_4]^{2-}$, were generated due to Coulomb's electrostatic forces of interaction according to Eq. (3) and thus more ZnO nuclei were produced. As the growth time further increased after nuclei formation, sheet defects initiated on the surfaces of newly formed ZnO nuclei, thereby increasing the radii of newly formed ZnO crystals as well as enlarging the phase boundaries of these crystals to the extent that they touched one another. As such, the base or core point of the flower-like structure was established (Fig. 1(c)). Once the basic structure was created, further growth in radial direction sprouted with exceeding reaction time to 30 min and these crystals developed into fully grown hierarchical flower-like assemblies which closely resembled with French marigold flower shape, given in the inset of Fig. 1(f). The steps of the proposed mechanism for the synthesis of uniform particles shown in Fig. 1(f) are schematically portrayed in Fig. 2.

It is generally accepted that in addition to the reaction time, other reaction parameters like pH of reactant solution and reaction temperature also affected the morphological features of the particle [17].

In this regard, a set of experiments were carried out in which pH of the reactant solution containing zinc nitrate and aqueous ammonia was kept below the isoelectric point of ZnO and the samples were heated for 10−30 min under reflux conditions. Figure 3 illustrates a fascinating morphological evolution under the effect of refluxing time and temperature. It was evident from the SEM images (Fig. 3(a)) that the powders obtained after 10 min refluxing time were composed of colloidal nanospheroids with excellent uniformity in particle shape and size. When the refluxing time was extended to 20 min, a considerable increase in particle size was observed with a slight change in particle morphology from spherical to oval shape with tapering ends (Fig. 3(b)). On further reflux heating (30 min), particles attained the shape of monodispersed ellipsoidal nanorods (Fig. 3(c)). The particles shown in Fig. 3 are schematically presented in Fig. 4.

In order to account for the above nanoparticle morphologies, it was noted during the synthesis that ZnO nanoparticles were probably formed through Reaction (3) when pH of the reactant mixture was below the PZC of the material. Therefore, they inhibited the expected homocoagulation during their growth stage due to highly positive charges on their surfaces and thus stayed smaller in size. According to BARUAH and DUTTA [17], at low pH, the nucleation rate was high, and the growth rate was slow due to fewer growth units formed. As a result, monodispersed fine particles of smaller sizes were produced. The morphological transformation into aesthetic nanorods evidenced that the reaction temperature was also responsible for controlling the particle morphology of the synthesized material. It was proposed that initially, the temperature of the reactant solution was low,

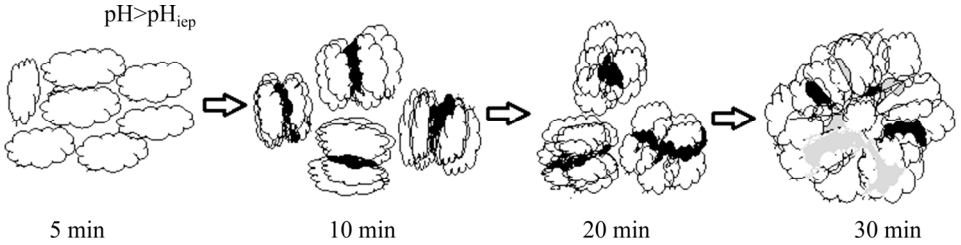

Fig. 2 Schematics illustrating effect of aging time on growth pattern of particles depicted in Fig. 1(f)

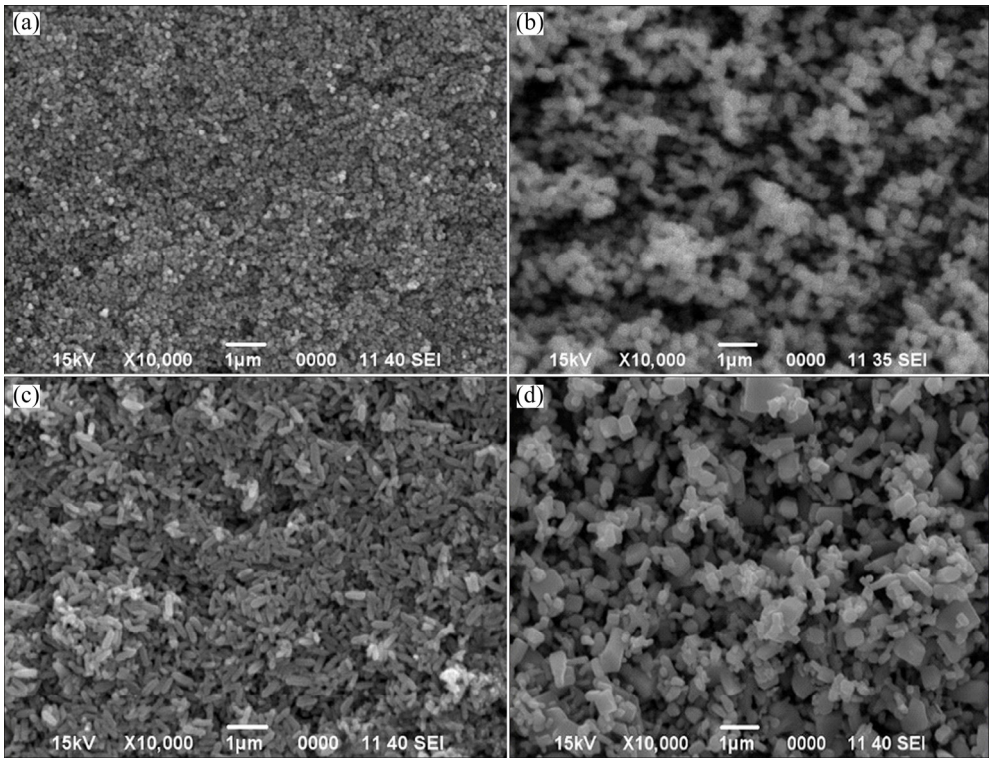

Fig. 3 SEM images of ZnO particles prepared using aqueous ammonia at different time intervals: (a) 10 min; (b) 20 min; (c) 30 min; (d) ZnO (commercial)

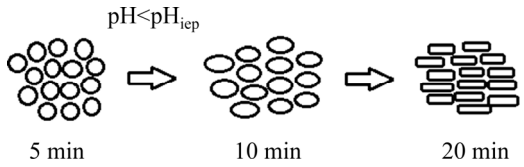

Fig. 4 Schematics illustration of growth mechanism of particles depicted in Figs. 3(a−c)

but the precipitated powder obtained sufficient thermal energy as the temperature of the reactant solution increased. It is added that these ellipsoidal ZnO nanorods formed through ammonia were much smaller and reported for the first time.

The present work employed a straightforward, time-effective and low-temperature aqueous synthesis route for obtaining uniform fine particles of ZnO without the addition of any surfactant. Though ZnO nano/micro flowers have been reported, the researchers either used higher temperatures with time requiring experimental procedures or they employed shaped directing additives like CETAB, monoethanolamine (MEA) and benzoic acid [18−20]. Similarly, ELKADY et al [21] employed various types of surfactants (CTAB, PEG, PVA and PVP) to construct ZnO particles with different particle morphologies.

Furthermore, selected batches of the synthesized particles, shown in Fig. 1(f) (nano-flowers) and Fig. 3(c) (nanorods), were used for further characterization by XRD, FTIR, and antibacterial analysis and labeled as ZnO-1 and ZnO-2, respectively. Also, to check the efficiency in antibacterial activity of the synthesized powders, a batch of commercial ZnO powder (ZnO-Com, Fig. 3(d)) was taken for antibacterial activity assay under the same conditions, and the results were compared.

3.1.2 XRD analysis

To confirm the composition and crystallinity, the selected batches of as-prepared particles were subjected to XRD analysis (Fig. 5). The XRD patterns of ZnO-1 and ZnO-2 were recorded over the 2θ range of 15°−80°. The presence of sharp diffraction peaks confirmed the fine crystalline nature of the synthesized particles. The acquired diffraction patterns matched well with the standard ICDD No. 50664. The observed peaks for both samples were indexed to wurtzite hexagonal phase of ZnO with characteristic reflection lines, identified as (100), (002), (112), (101), (102), (110), (103) and (200), respectively. The presence of

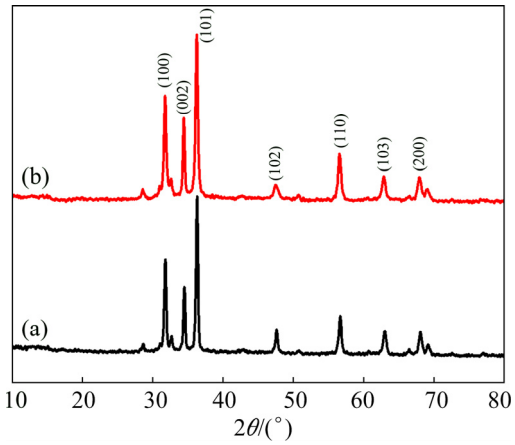

Fig. 5 XRD patterns of synthesized ZnO particles: (a) ZnO-1; (b) ZnO-2

similar diffraction peaks with different intensities on the two patterns can be attributed to the different crystallographic arrangement in these morphologies. For instance, the relative intensities of the peaks (100) and (101) were more significant for ZnO-2 with respect to ZnO-1. This, in fact, implied that the preferred orientations of crystals occurred during the growth stage. As can be seen in Fig. 5, no other peaks regarding the impurities or other crystalline phases were detected on the obtained XRD patterns, which confirmed the synthesized particles as pure crystalline ZnO. The diffraction data of the significant peaks of both XRD spectra were employed for estimation of the crystallite size of ZnO-1 and ZnO-2 by using Debye Scherrer formula [22]:

$$D=K\lambda/(\beta\cos\theta) \quad (5)$$

where D is crystallite size of the particles, K is Scherrer constant (0.9), λ is the wavelength of X-rays used (0.154 nm) and β is full width at half maximum of major diffraction peaks at the Bragg angle (θ).

The calculated average crystallite sizes were 11.92 and 17.55 nm for ZnO-1 and ZnO-2 (Table 1), respectively. The difference in crystallite sizes attributes to the degree of crystallinity of synthesized particle systems.

3.1.3 FTIR analysis

The same samples (ZnO-1 and ZnO-2) were also analyzed by FTIR spectroscopy to confirm the composition and purity of the synthesized product further. The FTIR spectra (Fig. 6) in the wave-number range of 400−4000 cm^{-1} were composed of several absorption bands, which appeared due to different vibrational frequencies of FTIR detectable various chemical groups present on the surfaces of test particles. The absorption bands in the region of 3800−3100 cm^{-1} were attributed to OH stretching vibrations [23,24]. Similarly, the bands at 1600−1400 cm^{-1} were due to the bending vibrations of OH [2].

Table 1 Crystallite size with respective diffraction peaks for synthesized ZnO samples

Sample	XRD peak	θ/rad	FWHM/rad	Crystallite size/nm	Average crystallite size/nm
ZnO-1	(100)	0.277	0.0148	9.76	11.92
	(002)	0.302	0.0101	14.30	
	(101)	0.314	0.0124	11.70	
ZnO-2	(100)	0.277	0.0086	16.79	17.55
	(002)	0.302	0.0087	16.60	
	(101)	0.314	0.0075	19.25	

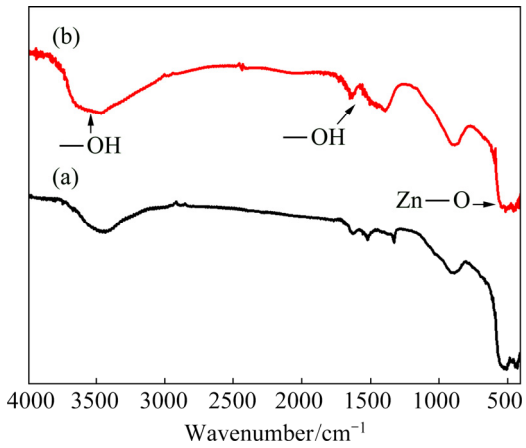

Fig. 6 FTIR spectra of synthesized ZnO particles: (a) ZnO-1; (b) ZnO-2

The occurrence of strong absorption bands at 527−423 cm^{-1} represented characteristic stretching vibrations of Zn—O bond, explicitly confirming the synthesized particles as pure ZnO [23]. The FTIR results thus supported Eqs. (2) and (4) for identifying the produced particles as pure ZnO.

3.2 Antibacterial activity assessment

For evaluation of the antibacterial activity, three samples of ZnO (ZnO-1, ZnO-2 and ZnO-Com) were investigated against various pathogenic bacteria, including two Gram-positive bacterial strains (*S. mutans* and *S. aureus*) and three Gram-negative bacterial strains (*E. coli*,

P. aeruginosa and *Enterobacter cloacae*). Agar well diffusion method was used and three different concentrations (0.25, 0.50 and 0.75 μg/μL) of the selected ZnO samples and positive control were employed. The presence of inhibition zones indicated the bactericidal property of the tested samples. The inhibitions zones produced by the tested ZnO samples against both Gram-positive and Gram-negative bacterial strains are illustrated in Figs. 7 and 8, respectively. The measured data are also recorded in Table 2. On the other side, ZnO-com showed no antibacterial activity in the employed concentration range (0.25−0.75 μg/μL). Figures 7 and 8 showed that the tested ZnO samples were potentially effective in suppressing the growth of the tested microorganism to variable potency, which can be examined clearly from the size of produced inhibition zones. It was, in fact, due to (1) the type of test bacteria, (2) the concentration of particles and (3) the morphology of the particles.

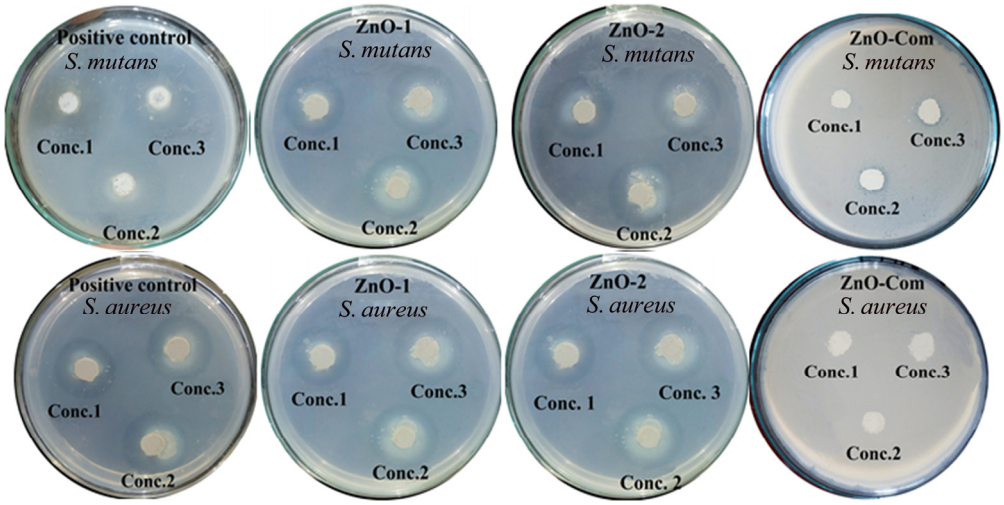

Fig. 7 Comparative antibacterial activity of ZnO and positive control against various Gram-positive bacterial strains (Conc.1—0.25 μg/μL; Conc.2—0.50 μg/μL; Conc.3—0.75 μg/μL)

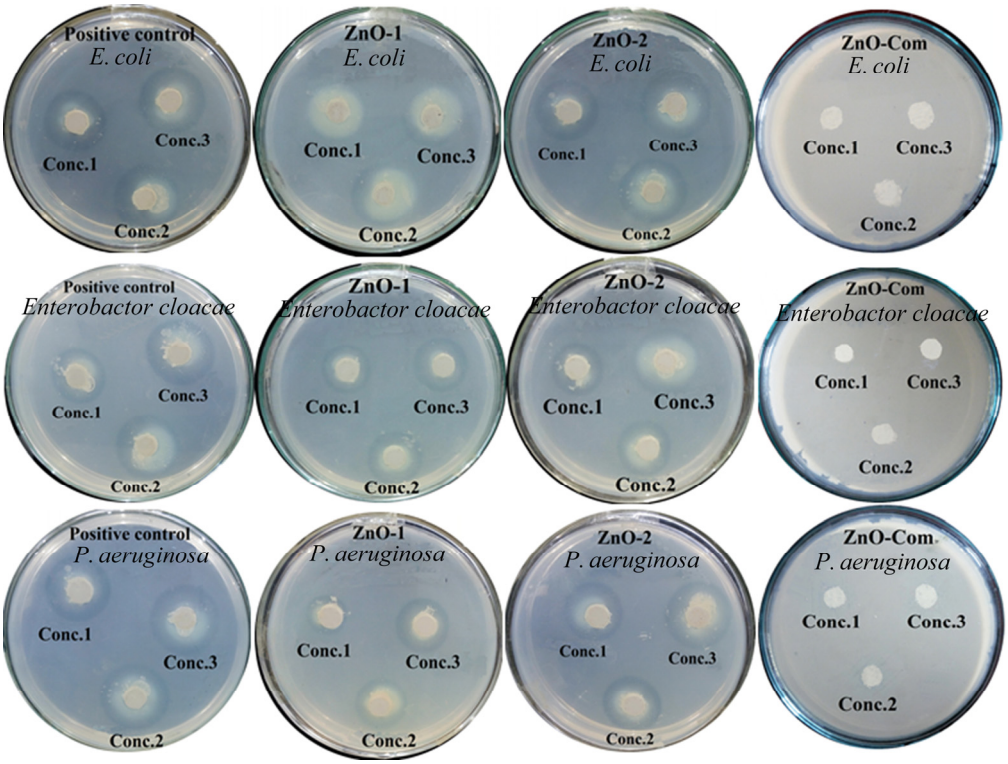

Fig. 8 Comparative antibacterial activity of ZnO and positive control against various Gram-negative bacterial strains (Conc.1—0.25 μg/μL; Conc.2—0.50 μg/μL; Conc.3—0.75 μg/μL)

Table 2 Antibacterial activity of ZnO against test bacterial strains

Bacterial strain	Zone of inhibition/mm								
	Sample 1			Sample 2			Positive control		
	0.25 μg/μL	0.50 μg/μL	0.75 μg/μL	0.25 μg/μL	0.50 μg/μL	0.75 μg/μL	0.25 μg/μL	0.50 μg/μL	0.75 μg/μL
S. mutans	28	29	31	30	32	33	31	33	34
S. aureus	28	30	31	29	30	32	30	32	34
E. coli	25	27	29	28	29	30	28	29	31
Enterobactor	24	25	27	25	26	28	25	27	29
P. aeruginosa	23	25	27	26	27	28	28	29	32

The diameters of inhibition zones increased with increasing the concentration of ZnO powder. These results revealed that the as-synthesized ZnO samples exhibited a promising antibacterial activity, which can be attributed to considerable uniformity in particle shape and size of the synthesized product.

From Table 2, it can be seen that the antibacterial activity of the test ZnO powders was comparable with the results shown by ciprofloxacin, used as a positive control. For instance, the bactericidal performance of ZnO has been improved by showing maximum inhibition zones at the concentration of 0.75 μg/μL as compared to the zone produced for 1.00 μg/μL employed by DOBRUCKA and DUGASZEWSKA [23]. Similarly, the size of inhibition zone observed in the present study for *S. aureus* was 30 mm, which was larger than that reported by MOSTAFA [25] (24.5 mm) for the same ZnO concentration (0.50 μg/μL). Furthermore, BAZANT et al [26] demonstrated that the antibacterial activity of pure ZnO increased (inhibition zone, 11−14 mm) for *S. aureus* with the addition of silver nanoparticles to ZnO.

Table 2 also shows that bactericidal activity was more toward Gram-positive than Gram-negative bacteria. This was because the antibacterial activity of NPs is also dependent upon the composition of the specific bacterial cell. Likewise, some researchers believed that the structure of the bacterial cell also affected the inhibitory action of the nanoparticles (NPs). For instance, due to the presence of a single membrane cell wall, Gram-positive bacteria were more susceptible to the antimicrobial action of ZnO [26]. Similarly, the thickness of the cell wall and certain other components of Gram-negative bacteria also affected the antimicrobial function of ZnO NPs.

The mechanism of the antibacterial activity of ZnO NPs has not been well understood so far. The antibacterial action is due to either one or a combination of the following proposed mechanisms: (1) production of reactive oxygen species (ROS), (2) toxic ions release, and (3) direct interaction of ZnO particles damage to cell membrane caused through adhesion of particles with the bacterial surface, and penetration through the cell membrane [27].

It is considered that the antibacterial action of ZnO through the well diffusion method was possibly due to the disruption of the cell membrane by direct interaction of ZnO particles with the bacterial surface. The direct contact might be due to the stress stimuli initiated by the particle shape, size, and surface charge of the particle, which resulted in electrostatic interaction between the ZnO particle and the surface of the bacterial cell. Such type of surface interaction was also confirmed by ZHANG et al [28] through the electrochemical measurements. On contact with the bacterial surface, reactive oxygen species were generated, which led to bacterial cell death by the chemical interaction of hydrogen peroxide with membrane proteins [11,28,29]. The direct damage to the cell membrane, thus, led to the leakage of the intracellular contents, causing the death of the bacterial cell.

4 Conclusions

(1) The synthesized zinc oxide (ZnO-1 and ZnO-2) demonstrated the promising antibacterial activity comparable to that of ciprofloxacin (positive control), while ZnO-Com showed no antibacterial response.

(2) The antibacterial activity of the as-prepared powders increased with the increasing concentration of ZnO (0.25−0.75 μg/μL).

(3) The inhibition zone was increased from ~30 to 33 mm against *Streptococcus mutans* and from ~28 to 30 mm against *Escherichia coli* for ZnO-2 nanoparticles. Besides, the antibacterial activity was more towards Gram-positive than Gram-negative bacteria.

(4) The synthesized uniform fine ZnO nanoparticles possess the great potential to be used as an antibacterial agent for inhibiting certain pathogenic bacteria.

Acknowledgments

The authors are thankful to the National Centre of Excellence in Physical Chemistry, University of Peshawar, Khyber Pakhtunkhwa, and the Higher Education Commission of Pakistan for facilitating this research study.

References

[1] GEETHA A, SAKTHIVEL R, MALLIKA J, KANNUSAMY R, RAJENDRAN R. Green synthesis of antibacterial zinc oxide nanoparticles using biopolymer azadirachta indica gum [J]. Oriental Journal of Chemistry, 2016, 32: 955−963.

[2] LUCILHA A C, SILVA M R, ANDO R A, DALL'ANTONIA L H, TAKASHIMA K. ZnO and Ag−ZnO crystals: Synthesis, characterization and application in heterogeneous photocatalysis [J]. Quimica Nova, 2016, 39: 409−414.

[3] GANESH S, NAVANEETHAN M, PATIL V L, PONNUSAMY S, MUTHAMIZHCHELVAN C, KAWASAKI S, PATIL P S, HAYAKAWA Y. Sensitivity enhancement of ammonia gas sensor based on Ag/ZnO flower and nanoellipsoids at low temperature [J]. Sensors and Actuators B, 2018, 255: 672−683.

[4] SUO Biao, LI Hua-rong, WANG Yue-xia, LI Zheng, PAN Zhi-li, AI Zhi-lu. Effects of ZnO nanoparticle-coated packaging film on pork meat quality during cold storage [J]. Journal of the Science of Food and Agriculture, 2017, 97: 2023−2029.

[5] GALSTYAN V, BHANDARI M P, SBERVEGLIERI V, SBERVEGLIERI G, COMINI E. Metal oxide nanostructures in food applications: Quality control and packaging [J]. Chemosensors, 2018, 6: 16−37. doi:10.3390/chemosensors 6020016.

[6] HATAMIE A, KHAN A, GOLABI M, TURNER A P F, BENI V, MAK W C M, SADOLLAHKHANI A, ALNOOR H, ZARGAR B, AZAM S, NUR O, WILLANDER M. Zinc oxide nanostructures modified textile and its application to biosensing, photocatalytic and as antibacterial material [J]. Langmuir, 2015, 31: 10913−10921.

[7] AKHTAR K, ZUBAIR N, IKRAM S, KHAN Z, KHALID H. Synthesis and characterization of ZnO nanostructures with varying morphology [J]. Bulletin of Material Science, 2017, 40: 459−466.

[8] MEMARZADEH K, SHARILI A S, HUANG J, RAWLINSON S C F, ALLAKER R P. Nanoparticulate zinc oxide as a coating material for orthopedic and dental implants [J]. Journal of Biomedical Materials Research: Part A, 2015, 103: 981−989.

[9] PALANIKUMAR L, RAMASAMY S, GOVINDASAMY H, BALACHANDRAN C. Influence of particle size of nano zinc oxide on the controlled delivery of *Amoxicillin* [J]. Applied Nanoscience, 2013, 3: 441−451.

[10] COLON G, WARD B C, WEBSTER T J. Increased osteoblast and decreased *Staphylococcus epidermidis* functions on nanophase ZnO and TiO_2 [J]. Juornal of Biomedical Materials Research: Part A, 2006, 78: 595−604.

[11] LIU Yue-jiao, HE Li-li, MUSTAPHA A, LI Haotiab, HU Zhi-qing, LIN Meng-shi. Antibacterial activities of zinc oxide nanoparticles against *Escherichia coli* O157:H7 [J]. Journal of Applied Microbiology, 2009, 107: 1193−1201.

[12] AZAM A, AHMED A S, OVES M, KHAN M S, HABIB S S, MEMIC A. Antimicrobial activity of metal oxide nanoparticles against Gram-positive and Gram-negative bacteria: A comparative study [J]. International Journal of Nanomedicine, 2012, 7: 6003−6009.

[13] THOMAS D, AUGUSTINE S, ABRAHAM J, THOMAS D T, PRAKASH J. In vitro antibacterial activity of ZnO nanoparticles prepared using sodium dodecyl sulfate as stabilizing agent [J]. Romanian Journal of Biophysics, 2015, 24: 295−303.

[14] HEZAM A, NAMRATHA K, DRMOSH Q, CHANDRASHEKAR B N, SADASIVUNI K K, YAMANI Z H, CHENG C, BYRAPPA K. Heterogeneous growth mechanism of ZnO nanostructures and the effects of their morphology on optical and photocatalytic properties [J]. Cryst Eng Comm, 2017, 19: 3299−3312.

[15] CHO Seungo, JUNG Seung-Ho, LEE Kun-Hong. Morphology-controlled growth of ZnO nanostructures using microwave irradiation: From basic to complex structures [J]. The Journal of Physical Chemistry C, 2008, 112, 12769−12776.

[16] BANFIELD J F, WELCH S A, ZHANG H Z, BERT T T, PENN R L. Aggregation-based crystal growth and microstructure development in natural iron oxyhydroxide biomineralization products [J]. Science, 2000, 289: 751−754

[17] BARUAH S, DUTTA J. pH-dependent growth of zinc oxide nanorods [J]. Journal of Crystal Growth, 2009, 311: 2549−2554.

[18] ZHANG Hui, YANG De-ren, JI Yu-jie, MA Xiang-Yang, XU Jin, QUE Duan-lin. Low temperature synthesis of flowerlike ZnO nanostructures by cetyltrimethylammonium bromide-assisted hydrothermal process [J]. The Journal of Physical Chemistry B, 2004, 108: 3955−3958.

[19] HUSSAIN S, LIU T, KASHIF M, LIN Liang, WU Shu-fang, GUO Wei-wei, ZENG Wen, HASHIM U. Effects of reaction time on the morphological, structural, and gas sensing properties of ZnO nanostructures [J]. Materials Science in Semiconducting Processing, 2014, 18: 52−58.

[20] GAO Xiao-qing, ZHAO Hua, WANG Ji-de, SU Xin-tai, XIAO Feng. Morphological evolution of flower-like ZnO

microstructures and their gas sensing properties [J]. Ceramic International, 2013, 39: 8629−8632.

[21] ELKADY M, HASSAN H S, HAFEZ E E, AHMED F. Construction of zinc oxide into different morphological structures to be utilized as antimicrobial agent against multidrug resistant bacteria [J]. Bioinorganic Chemistry and Applications, 2015, 5: 1−20.

[22] MOHAMMED O D A, MUSTAFA A M. Synthesis and characterization of zinc oxide nanoparticles using zinc acetate dihydrate and sodium hydroxide [J]. Journal of Nanoscience and Nanoengineering, 2015, 1: 248−251.

[23] DOBRUCKA R, DUGASZEWSKA J. Biosynthesis and antibacterial activity of ZnO nanoparticles using *Trifolium pretense* flower extract [J]. Saudi Journal of Biological Sciences, 2016, 23: 517−523.

[24] GOUDARZI M, MOUSAVI KAMAZANI M, SALAVATI N M. Zinc oxide nanoparticles: Solvent-free synthesis, characterization and application as heterogeneous nanocatalyst for photodegradation of dye from aqueous phase [J]. Journal of Materials Science: Materials in Electronics, 2017, 28: 8423−8428.

[25] MOSTAFA A A. Antibacterial activity of zinc oxide nanoparticles against toxigenic *bacillus cereus*and *staphylococcus aureus* isolated from some egyptian food [J]. International Journal of Microbiological Research, 2015, 6: 145−154.

[26] BAZANT P, KLOFAC J, MUNSTER L, KURITKA I. Antibacterial powders for medical application prepared by microwave hydrothermal assisted synthesis [J]. Nanoscience and Nanotechnology, 2016, 6: 88−91.

[27] BAZANT P, KURITKA I, MUNSTER L, MACHOVSKY M, KOZAKOVA Z, SAHA P. Hybrid nanostructured Ag/ZnO decorated powder cellulose fillers for medical plastics with enhanced surface antibacterial activity [J]. Journal of Materials Science: Materials in Medicine, 2014, 25: 2501−2512.

[28] ZHANG Ling-ling, JIANG Yun-hong, DING Yu-long, DASKALAKIS N, JEUKEN L, POVEY M, O'NEILL A J, DAVID W Y. Mechanistic investigation into antibacterial behaviour of suspensions of ZnO nanoparticles against *E. coli* [J]. Journal of Nanoparticle Research, 2010, 12: 1625−1636.

[29] SHARMA D, RAJPUT J, KAITH B S, KAUR M, SHARMA S. Synthesis of ZnO nanoparticles and study of their antibacterial and antifungal properties [J]. Thin Solid Films, 2010, 519: 1224−1229.

氧化锌纳米颗粒的形貌控制合成及其体外抗菌活性

Naila ZUBAIR, Khalida AKHTAR

National Center of Excellence in Physical Chemistry, University of Peshawar,
Peshawar-25120, Khyber Pukhtoonkhwa, Pakistan

摘　要：在不使用任何表面活性剂或模板的情况下，采用可控沉淀法在水溶液中成功合成形貌均匀的分层花状和纳米棒状氧化锌(ZnO)。为了阐明纳米颗粒的生长机理，系统研究 pH、反应时间和温度对纳米颗粒形貌的影响。采用 SEM、FT-IR 和 XRD 等表征手段对样品进行分析。 XRD 谱证实合成的粉末具有良好的结晶性。此外，对比研究合成的花状(ZnO-1)和纳米棒状(ZnO-2)的 ZnO 纳米颗粒与商业 ZnO(ZnO-Com)颗粒的体外抗菌活性。结果表明，在实验条件下，ZnO-2 比 ZnO-1 对受试菌具有更高的抗菌活性，而商业 ZnO 则没有抗菌活性。当 ZnO-2 的浓度从 0.25 升高到 0.75 μg/μL 时，对变异链球菌的抑菌环从约 30 mm 扩大到 33 mm，对大肠杆菌的抑菌环从约 28 mm 增大到 30 mm。研究表明，合成的氧化锌纳米颗粒作为抗菌剂，可能在生物医学方面有效抑制某些致病菌。

关键词：ZnO；纳米颗粒；菌株；抗菌活性

(Edited by Bing YANG)